RSC Advances

PAPER

View Article Online
View Journal | View Issue

Cite this: *RSC Adv.*, 2025, **15**, 37027

Polyacrylamide functionalized polysaccharide based nanocomposite semi-interpenetrating polymeric network hydrogel for pH-responsive controlled release of a model neuroprotective drug

Nada H. Aljarba,[a] Mohd Afzal, *[b] Mariam Abdulaziz Alkhateeb[a] and Saad Alkahtani[c]

The development of advanced drug delivery systems with enhanced stability, controlled release, and biocompatibility is critical for effective neuroprotective therapies. Here, we report a polyacrylamide-functionalized polysaccharide-based nanocomposite semi-interpenetrating polymer network (semi-IPN) hydrogel designed for pH-responsive delivery of the neuroprotective agent citicoline. The semi-IPN structure provides enhanced mechanical strength and tunable swelling, enabling precise and sustained pH-responsive drug release while minimizing burst effects. SEM analysis revealed a porous microstructure that facilitates efficient drug loading and diffusion, and XRD confirmed a semi-crystalline architecture contributing to mechanical stability. Cytotoxicity studies using 3T3 fibroblasts demonstrated excellent biocompatibility, with proliferation comparable to the control. Collectively, these results demonstrate that the developed hydrogel combines robust mechanical properties, tunable swelling, and controlled drug release, representing a promising platform for targeted and effective neuroprotective therapy.

Received 18th August 2025
Accepted 24th September 2025

DOI: 10.1039/d5ra06115f

rsc.li/rsc-advances

Introduction

The development of smart drug delivery systems has become a focal point in pharmaceutical research, particularly for the controlled and targeted release of bioactive molecules.[1] Among these systems, hydrogels have emerged as versatile platforms due to their ability to retain large quantities of water, biocompatibility, and tunable physical properties.[2] Hydrogels are three-dimensional polymeric networks capable of undergoing reversible volume changes in response to external stimuli such as pH, temperature, and ionic strength.[3–6] These characteristics make hydrogels ideal for controlled drug delivery applications, especially in systems requiring precise release kinetics and environmental responsiveness.[7] In recent years, polysaccharide-based hydrogels have attracted considerable attention in biomedical applications due to their natural abundance, biodegradability, and inherent bioactivity.[8–10] Polysaccharides such as chitosan, alginate, and cellulose derivatives have demonstrated excellent film-forming ability, mucoadhesiveness, and non-toxicity, making them suitable candidates for sustained drug release.[11–13] Chitosan, in particular, has shown remarkable potential for pH-sensitive systems due to its cationic nature, enabling it to swell in acidic environments and shrink under neutral or alkaline conditions.[14] pH-Responsive hydrogels are widely employed in controlled drug delivery due to their ability to alter swelling behavior and drug diffusion in response to changes in environmental pH. Such systems are particularly relevant in pathological conditions where local pH differs from normal physiological levels.[15] For instance, ischemic or inflamed brain regions often exhibit slightly acidic microenvironments, which can affect drug availability and therapeutic efficacy. By designing hydrogels that respond to these pH changes, it is possible to achieve site-specific and controlled release of neuroprotective agents, such as citicoline, thereby enhancing their therapeutic potential while minimizing systemic side effects.[16,17] Meanwhile, alginate hydrogels have exhibited pH-dependent gelation behavior, further expanding their use in targeted drug delivery systems.[18] Recent studies have highlighted their potential in tissue regeneration, such as high-toughness adaptive hydrogels for remodeling the growth plate in children *via* IGF-I delivery.[19] Hydrogels have also been explored for dental applications, including the treatment of dental caries,[20] and for cartilage repair through injectable hydrogel microspheres.[21] Moreover, bio-adhesive hydrogels with antibacterial properties show promise in managing periodontal diseases.[22] These examples underscore the broad applicability of hydrogel systems and motivate the design of functional hydrogels for controlled drug delivery in

[a]*Department of Biology, College of Sciences, Princess Nourah bint Abdulrahman University, P. O. Box 84428, Riyadh 11671, Saudi Arabia*

[b]*Department of Chemistry, College of Science, King Saud University, P. O. Box 2455, Riyadh 11451, Saudi Arabia. E-mail: maslam1@ksu.edu.sa*

[c]*Department of Zoology, College of Science, King Saud University, P. O. Box 2455, Riyadh 11451, Saudi Arabia*

neuroprotective therapies. Despite these advantages, polysaccharide-based hydrogels alone often suffer from poor mechanical strength, rapid degradation, and limited control over drug release profiles, necessitating structural modifications or hybrid designs.[23,24] To overcome these limitations, the incorporation of synthetic polymers such as polyacrylamide (PAAm) has been explored to improve the mechanical stability and responsiveness of hydrogel systems. PAAm is a hydrophilic, non-toxic polymer known for its excellent mechanical strength, flexible crosslinking characteristics, and tunable water retention properties.[25–27] When integrated into a hydrogel matrix, PAAm contributes to enhanced stability, improved swelling behavior, and extended drug release profiles. Several studies have successfully demonstrated PAAm-based hybrid hydrogels in various biomedical applications.[28,29] For instance, PAAm–chitosan hybrid hydrogels have been employed for the controlled release of anti-inflammatory agents, while PAAm–alginate composites have shown promise for sustained anticancer drug delivery.[30–32]

Semi-interpenetrating polymer networks (semi-IPNs) have emerged as a promising hydrogel design strategy to combine the unique properties of both natural and synthetic polymers.[33] A semi-IPN structure allows one polymer (usually the natural polymer) to remain linear or branched within a crosslinked polymeric network (typically the synthetic polymer).[34–36] This configuration leverages the bioactivity and swelling behavior of the natural polymer while benefiting from the mechanical reinforcement provided by the synthetic polymer.[37] Recent advancements in semi-IPN hydrogels have enabled improved drug encapsulation efficiency, sustained release behavior, and better structural integrity for prolonged biomedical applications.[38]

Nootropic and neuroprotective drugs; which are designed to enhance cognitive function and protect against neurological damage, require precise delivery systems to achieve optimal therapeutic outcomes.[39,40] Conventional delivery methods often struggle with issues such as burst release, poor bioavailability, and limited blood–brain barrier penetration.[41] Machine learning and artificial intelligence approaches can support the development of hydrogel formulations for neuroprotective and nootropic drug delivery by analyzing physicochemical properties and patient- or disease-specific data,[42–44] enabling more precise, controlled, and potentially personalized therapeutic strategies.[45,46] pH-Responsive hydrogel systems provide a promising strategy to overcome these challenges by enabling site-specific drug release in response to physiological pH variations, thereby enhancing drug stability, bioavailability, and targeted delivery to neural tissues.[47] In this study, we present a novel polyacrylamide-functionalized polysaccharide-based semi-IPN hydrogel system designed specifically for pH-responsive, controlled delivery of nootropic and neuroprotective drugs. This hybrid design combines the biodegradable and bioactive properties of polysaccharides with the mechanical robustness of PAAm, resulting in a hydrogel system with improved mechanical strength, tailored swelling behavior, and prolonged drug release capabilities. The proposed hydrogel design guarantees the safety and stability of nootropic medications while enabling their controlled release in accordance with physiological pH fluctuations, specifically aimed at areas like the gastrointestinal tract or the blood–brain barrier. This study integrates biocompatible materials with a customized semi-IPN structure to tackle obstacles in neuroprotective drug delivery systems, representing a substantial advancement in the creation of effective, responsive treatment platforms for neurological illnesses.

Materials and methods

Materials

Starch (from potato, tested according to Ph. Eur.) was purchased from Sigma, Germany and used as received. Acrylamide acid (AAm), lithium phenyl-2,4,6-trimethylbenzoylphosphinate (LAP), *N*,*N*-methylenebisacrylamide (MBA) were purchased from the Sigma. Montmorillonite K10 (MMT, 220–270 $m^2\ g^{-1}$) was procured from Sigma, Germany. The citicoline sodium obtained from Biosans Lifecare, Kandivali, Mumbai, India, was utilized as received. Other chemicals used here are of analytical grades and used without any further purifications.

Synthesis of nanocomposite hydrogel (NCHG)

The nanocomposite hydrogel (NCHG) was synthesized using a UV-triggered free radical polymerization technique. Initially, 1 g of starch was dispersed in 50 mL of deionized water and heated to 70 °C with continuous stirring on a magnetic hotplate to ensure complete dissolution. A specific amount of MMT (1–3 wt%) was added to the solution and sonicated for 30 minutes. The resulting homogeneous solution was cooled to room temperature before adding 2 g of acrylamide (AAm), which was stirred vigorously for 20 minutes to achieve uniform mixing. To facilitate crosslinking, 0.05 g of MBA was introduced as a crosslinker and stirred for an additional 10 minutes. Subsequently, 0.02 g of LAP was added to the solution as a photoinitiator, and the mixture was stirred for 5 minutes to ensure complete dispersion.

The prepared solution was transferred into pre-cleaned molds with dimensions of approximately 3 cm × 3 cm × 0.5 cm to maintain consistent hydrogel thickness. The molds were placed in a UV chamber and exposed to 365 nm UV light for 30 minutes to initiate the polymerization process. The crosslinked hydrogel was removed from the mold and rinsed thoroughly with deionized water to eliminate any unreacted monomers, crosslinkers, or by-products. The purified hydrogel samples were then frozen at −20 °C for 24 hours before being subjected to freeze-drying at −50 °C for 48 hours to obtain the final nanocomposite hydrogel (NCHG) in a dry, stable form suitable for characterization and further application.

Results and discussions

The successful synthesis of the NCHG was confirmed through the visual and structural insights presented in Fig. 1. The schematic illustrates the UV-triggered free radical gelation

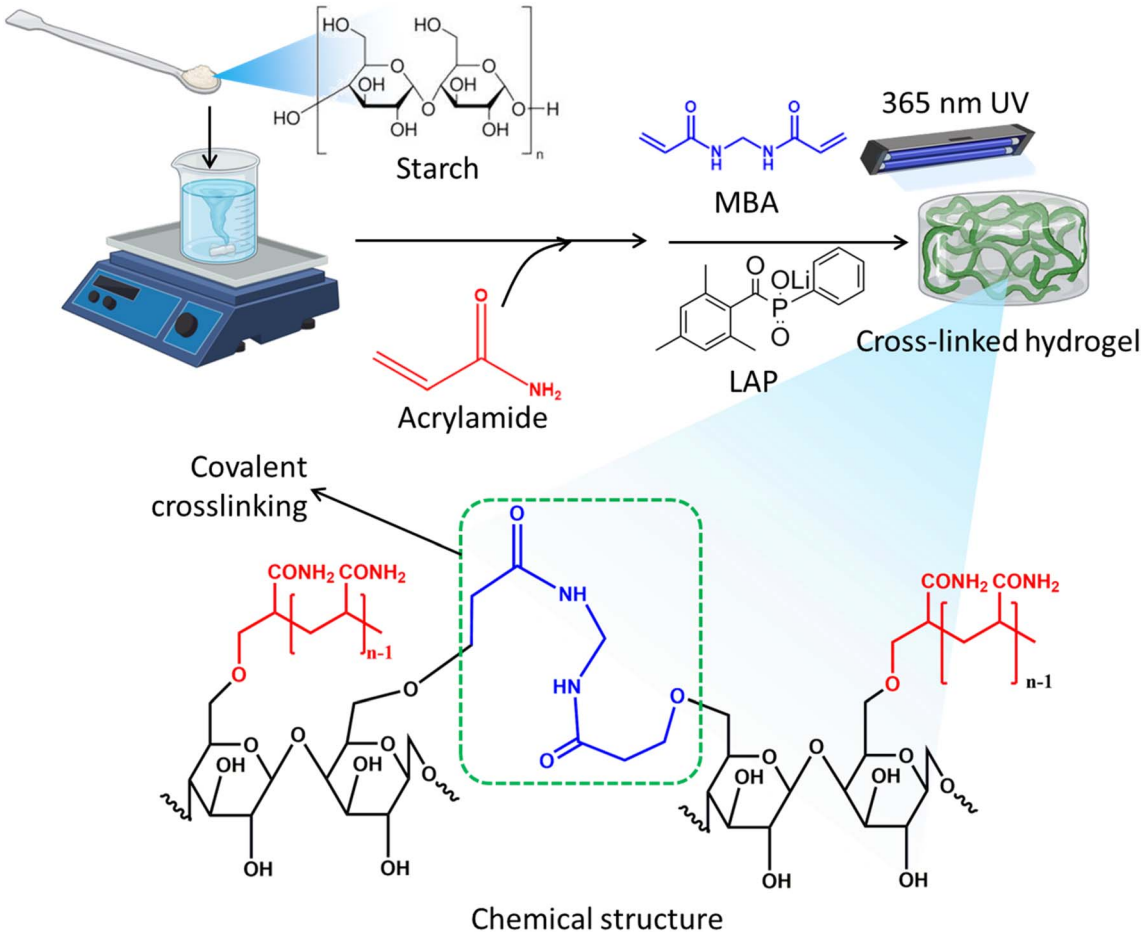

Fig. 1 Schematic of UV triggered hydrogel preparation by free radical gelation technique.

technique used for hydrogel preparation, highlighting the critical steps and chemical interactions involved. The formation of the hydrogel matrix relied on the integration of starch and acrylamide monomers *via* covalent crosslinking facilitated by MBA under 365 nm UV irradiation. Starch, a polysaccharide rich in hydroxyl groups, offered a hydrophilic framework that improved water retention and mechanical strength. The presence of acrylamide ensured the formation of a polyacrylamide network within the starch matrix, creating a semi-IPN structure. This configuration improved the structural robustness of the hydrogel while maintaining its flexibility and responsiveness to external stimuli. The role of LAP as the photoinitiator was crucial in generating reactive free radicals under UV irradiation, which initiated the polymerization of acrylamide. The diagram explicitly depicts the covalent bond between the starch matrix and polyacrylamide chains, guaranteeing the development of a highly linked, mechanically robust hydrogel structure. The presence of amide groups ($-CONH_2$) in the polymer network further contributed to hydrogen bonding interactions, reinforcing the mechanical properties and ensuring pH-responsive behavior. The chemical structure depiction reveals distinct segments of the hydrogel network: starch chains (black), polyacrylamide chains (red), and MBA-linked covalent crosslinking units (blue) (Fig. 1). This interconnected architecture is expected to provide enhanced swelling capacity, stability under physiological conditions, and controlled drug release profiles, especially for nootropic and neuroprotective agents.

Characterizations of nanocomposite hydrogels

The structural characteristics of the produced nanocomposite hydrogel (NCHG) were examined utilizing FTIR and NMR spectroscopy (Fig. 2). The FTIR spectra (Fig. 2a) exhibited notable alterations in the typical peaks, validating the effective synthesis of the nanocomposite hydrogel. Pure starch exhibited a prominent O–H stretching vibration at 3365 cm^{-1} and C–H stretching at 2932 cm^{-1}.[48] After the addition of acrylamide and subsequent crosslinking, the appearance of a distinct peak at 1680 cm^{-1} in NCHG confirmed the presence of C=O stretching vibrations from amide groups, characteristic of polyacrylamide.[49] The shifting of the O–H band to 3348 cm^{-1} in NCHG indicated hydrogen bonding interactions between starch and the acrylamide network. Additionally, the presence of a peak at 3632 cm^{-1} in MMT confirmed the characteristic silicate structure.[50] The reduced intensity of the starch peak at 3365 cm^{-1} and the appearance of new peaks in NCHG collectively validate the successful formation of the nanocomposite

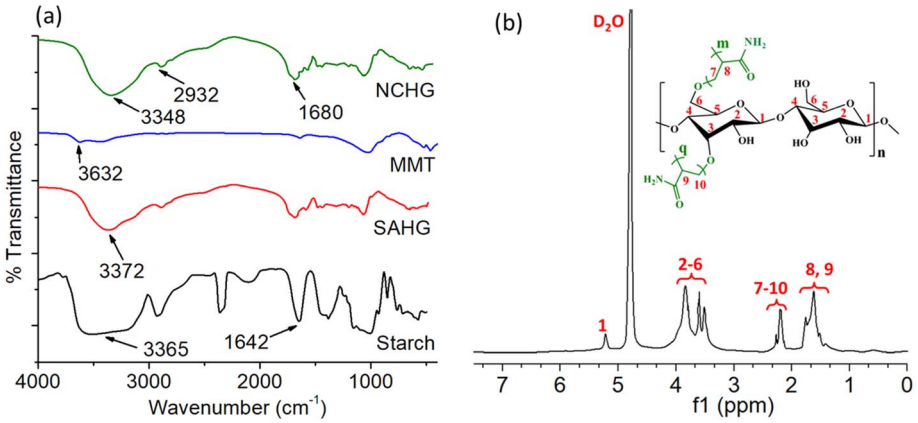

Fig. 2 (a) FTIR spectra of pure starch, MMT and the prepared nanocomposite hydrogel. (b) NMR spectrum of the starch-polyacrylamide system confirming the polyacrylamide grafting onto starch.

hydrogel.[51] The NMR spectrum (Fig. 2b) further confirmed the polyacrylamide grafting onto the starch backbone. The proton resonance peak observed at 1 ppm corresponds to the terminal methyl protons of the starch backbone. The peaks between 2–6 ppm represent the methylene ($-CH_2-$) protons from the polyacrylamide chains, confirming successful polymerization. Notably, peaks appearing between 7–10 ppm indicate the presence of amide protons ($CONH_2$) in the polymer network, reinforcing the formation of a stable polyacrylamide–starch structure.[52] The combined FTIR and NMR results strongly support the successful synthesis and structural integrity of the nanocomposite hydrogel.

The X-ray diffraction (XRD) analysis shown in Fig. 3 reveals the structural transformation occurring in pristine starch and the synthesized nanocomposite hydrogels (NCHG1, NCHG2, and NCHG3). The pristine starch sample exhibits characteristic sharp peaks at approximately 17.1°, 19.8°, and 22.9° in the 2θ range, which are typical of the semi-crystalline nature of starch. These peaks confirm the presence of well-ordered crystalline domains within the starch structure, resulting from hydrogen bonding among starch polymer chains.[53] Upon the formation of nanocomposite hydrogels, significant changes in the XRD patterns are evident. The diffraction peaks in NCHG1, NCHG2, and NCHG3 are significantly broader and less intense than those of pristine starch. The widening and decrease in intensity signify a disturbance in the inherent crystalline structure of starch during the hydrogel production process. The grafting of polyacrylamide chains and crosslinking reactions likely disturbed the ordered arrangement of starch molecules, transforming the material into a more amorphous phase. Among the three nanocomposite hydrogel samples, NCHG3 exhibits the most pronounced broadening and intensity reduction, suggesting a higher degree of crosslinking or polymer incorporation.[54] Conversely, NCHG1 retains relatively more of its crystalline features, indicating a lower degree of disruption. These observations suggest that increasing polymer content or crosslinking density progressively diminishes the crystallinity of the system, enhancing the amorphous nature of the hydrogel network. The reduction in crystallinity generally correlates with improved swelling capacity, enhanced water retention, and better mechanical flexibility; key attributes for controlled drug delivery applications.[55] The observed structural changes confirm successful modification of starch into a nanocomposite hydrogel with tunable crystallinity depending on the formulation parameters.

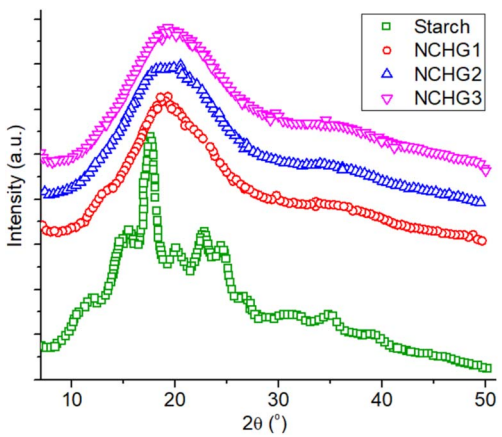

Fig. 3 XRD of pristine starch, and starch based nanocomposite hydrogels.

The scanning electron microscopic (SEM) images presented in Fig. 4 depict the surface morphology of the nanocomposite hydrogels NCHG1, NCHG2, and NCHG3. These micrographs reveal distinct textural and structural features that provide insights into the porosity, surface roughness, and interconnected network formation of the hydrogel systems. The SEM picture of all the nanocomposite hydrogels reveals a comparably dense surface with fewer discernible pores. The restricted porosity indicates a diminished level of crosslinking or polymer integration, perhaps limiting the water absorption capacity and flexibility of this sample. The compact morphology indicates a more ordered internal structure with minimal void spaces. Such morphology is particularly desirable in biomedical applications such as drug delivery, where efficient fluid transport and molecular diffusion are critical.[56] Inclusive, the SEM analysis

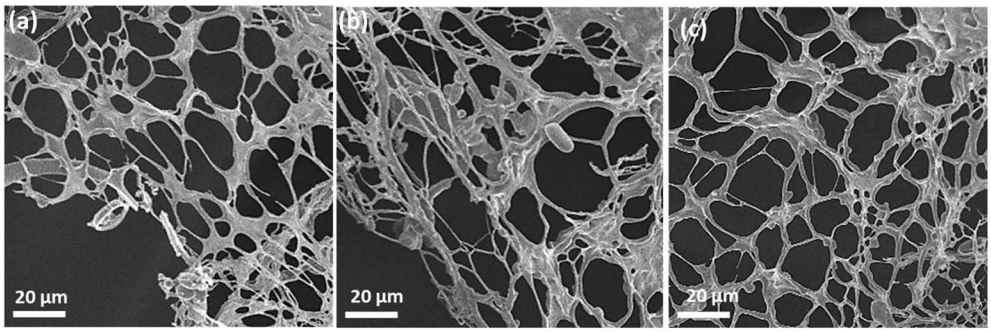

Fig. 4 Scanning electron microscopic images of the starch based semi-IPN nanocomposite hydrogel having significant porosities of (a) NCHG1; (b) NCHG2; (c) NCHG3.

confirms that the nanocomposite hydrogels possess tunable porosity, with NCHG3 exhibiting the most desirable structure for enhanced fluid diffusion and potential application in drug delivery systems or tissue engineering scaffolds.

The rheological analysis of the hydrogels, as illustrated in Fig. 5, provides crucial insights into their mechanical stability, viscoelastic behavior, and structural integrity, which are essential parameters for their potential application in pH-responsive nootropic and neuroprotective controlled drug delivery. The frequency sweep test (Fig. 5a) reveals that the storage modulus (G') of all hydrogel formulations increases with frequency, indicating a dominant elastic behavior over viscous behavior. Among the tested formulations NCHG3 exhibits the highest G' values suggesting enhanced crosslinking density and reinforcement due to nanocomposite integration.[57] The improvement in mechanical strength is attributed to the incorporation of functionalized polysaccharides, which introduce additional hydrogen bonding and electrostatic interactions, thereby improving the gel network's elasticity and mechanical resilience. The stress sweep test (Fig. 5b) further demonstrates the hydrogels' structural robustness under increasing shear stress. A critical point is observed where the G' value sharply decreases, indicating the rupture of the gel network.[58] Notably, the HG (without starch) hydrogel collapses at a lower shear stress compared to nanocomposite-reinforced hydrogels, confirming the role of polysaccharide-based reinforcements in delaying network failure. NCHG3 endures the greatest shear stress among the formulations; supporting the concept that functionalization improves the semi-IPN structure. The prolonged stability under stress indicates that these nanocomposite hydrogels can preserve their structural integrity in physiological conditions, which is essential for controlled drug release applications.

The thermal stability of the pristine starch, montmorillonite (MMT), and nanocomposite hydrogels was evaluated through Differential Scanning Calorimetry (DSC) and Thermogravimetric Analysis (TGA), as illustrated in Fig. 6. The DSC curves (Fig. 6a) reveal the glass transition temperature (T_g) shift upon the incorporation of MMT, highlighting the structural reinforcement imparted by nanocomposite integration. Pristine starch exhibits a T_g around 100–120 °C, attributed to the disruption of hydrogen bonding and moisture evaporation.[59] However, after the inclusion of MMT, the nanocomposite hydrogels exhibit a noticeable T_g shift to higher temperatures (~140–160 °C for NCHG3), indicating increased polymer chain rigidity and reduced molecular mobility due to strong polymer–nanofiller interactions. This enhancement in thermal stability is further validated by TGA analysis (Fig. 6b), which

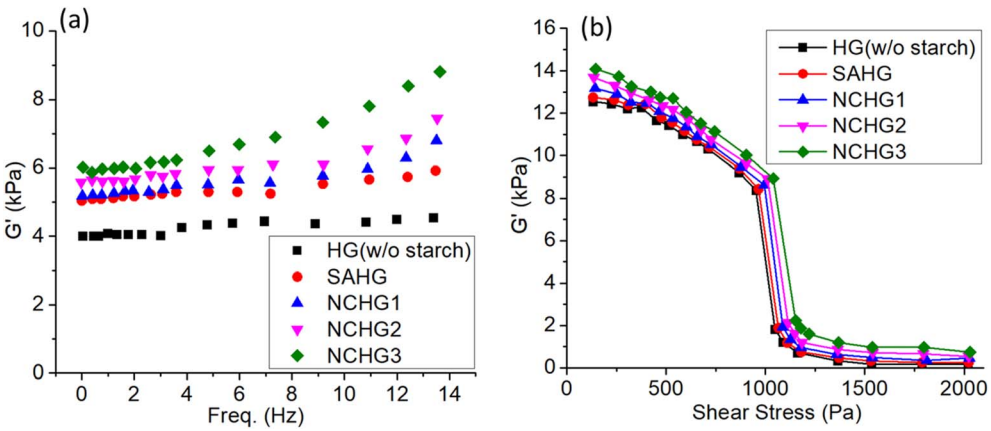

Fig. 5 (a) Frequency dependent rheological behavior of different hydrogels (b) stress sweep experimental study of the hydrogels showing point of rupture and delayed network breaking as a function of reinforcements.

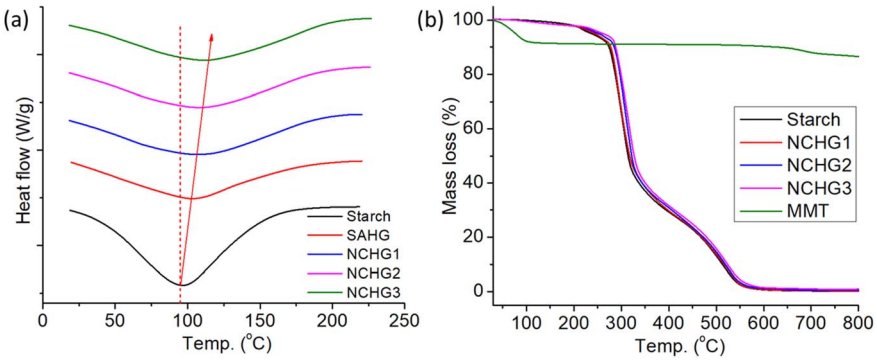

Fig. 6 (a) DSC of pristine starch and the hydrogels. (b) TGA plot of pristine starch, MMT, and nanocomposite hydrogels.

demonstrates a delayed thermal degradation onset for the nanocomposite hydrogels compared to pristine starch.[60] The major decomposition stage for pristine starch occurs around 280–350 °C, while the nanocomposite hydrogels show a shift to ~320 °C, with NCHG3 exhibiting the highest thermal resistance. Additionally, the higher residual mass (~15%) at 800 °C for NCHG3 confirms its superior char formation, reinforcing the role of MMT as a thermal stabilizer.[61] The findings confirm that the inclusion of MMT markedly improves the structural integrity of semi-IPN hydrogels, rendering them viable options for pH-responsive controlled drug administration, where maintaining stability under physiological and thermal stress is crucial.

The water uptake and swelling behavior of the prepared hydrogels were systematically evaluated, as illustrated in Fig. 7, to assess their responsiveness to different environmental factors, which is crucial for controlled drug delivery applications. The bar chart (Fig. 7a) compares the equilibrium swelling ratio (SR) of the unfilled hydrogel (SAHG) and nanocomposite hydrogels. The SAHG hydrogel exhibits the highest swelling ratio (~22), whereas the swelling ratio decreases with increasing nanocomposite content (NCHG3 showing the lowest at ~15). This reduction is attributed to the enhanced crosslinking density and strong polymer–nanofiller interactions, which restrict water absorption by limiting the expansion of the hydrogel matrix.[62] The time-dependent swelling behavior (Fig. 7b) further confirms this trend, showing a rapid initial water uptake phase followed by saturation. The SAHG hydrogel reaches equilibrium swelling within ~1500 minutes, while the nanocomposite hydrogels exhibit a slower uptake due to nanofiller-induced network rigidity.[63] The first-order rate kinetic analyses (Fig. 7c) indicate the kinetic regulation of water absorption, with SAHG exhibiting the largest swelling rate, succeeded by NCHG1, NCHG2, and NCHG3. The reduced swelling rates of nanocomposite hydrogels suggest that the inclusion of MMT enhances the mechanical strength and stability of the hydrogels, rendering them more appropriate for prolonged drug release as opposed to instantaneous burst release.

The pH-dependent swelling behavior (Fig. 7d) of NCHG2 highlights its pH-responsive nature, essential for targeted drug release in different physiological environments. The swelling ratio (SR) is lowest at pH ~2 (~5), gradually increases to a maximum (~20) at pH ~9, and decreases again at alkaline pH (~10–12). This behavior suggests that the hydrogel exhibits anionic characteristics, where protonation and deprotonation of functional groups influence the electrostatic interactions and hydration capacity.[64] This makes NCHG2 highly suitable for targeted drug release in the intestinal region (pH ~ 7–9) rather than the stomach (pH ~ 1–3). Finally, the salinity-dependent swelling behavior (Fig. 7e) of NCHG2 was evaluated in the presence of different ionic species. The swelling ratio decreases significantly with increasing salt concentration, following the trend $K^+ > Na^+ > Ba^{2+} > Ca^{2+} > Mg^{2+}$. This can be explained by ionic crosslinking effects, where divalent cations (Ba^{2+}, Ca^{2+}, and Mg^{2+}) induce stronger electrostatic interactions within the hydrogel matrix, reducing water absorption.[65] The pronounced decrease in swelling at higher salt concentrations (~50% reduction at 1.2 wt%) suggests that NCHG2 is highly sensitive to ionic strength, an important factor for real-world physiological applications where salt concentration fluctuations can modulate drug release profiles.

Mechanical properties

The mechanical properties of the synthesized polyacrylamide-functionalized polysaccharide-based nanocomposite hydrogel were evaluated through tensile and compressive stress–strain measurements, as shown in Fig. 8. The results demonstrate a clear enhancement in mechanical strength with the inclusion of montmorillonite (MMT) nanocomposites, confirming the formation of a robust semi-IPN structure. In the tensile stress–strain plot (Fig. 8a), the SAHG sample exhibited a maximum strain of approximately 1200% before fracture, with a corresponding tensile stress of ~0.045 MPa. The nanocomposite hydrogels showed progressively improved tensile strength and elongation at break with increasing MMT content. Notably, NCHG3 achieved the highest tensile stress (~0.07 MPa) and strain limit (~1000%) among all samples. This enhanced tensile behavior can be attributed to the strong interfacial interactions between the polymer chains and MMT nanosheets, which effectively reinforced the hydrogel matrix. The improved mechanical properties confirm the effective dispersion of MMT within the hydrogel, forming a physically crosslinked network

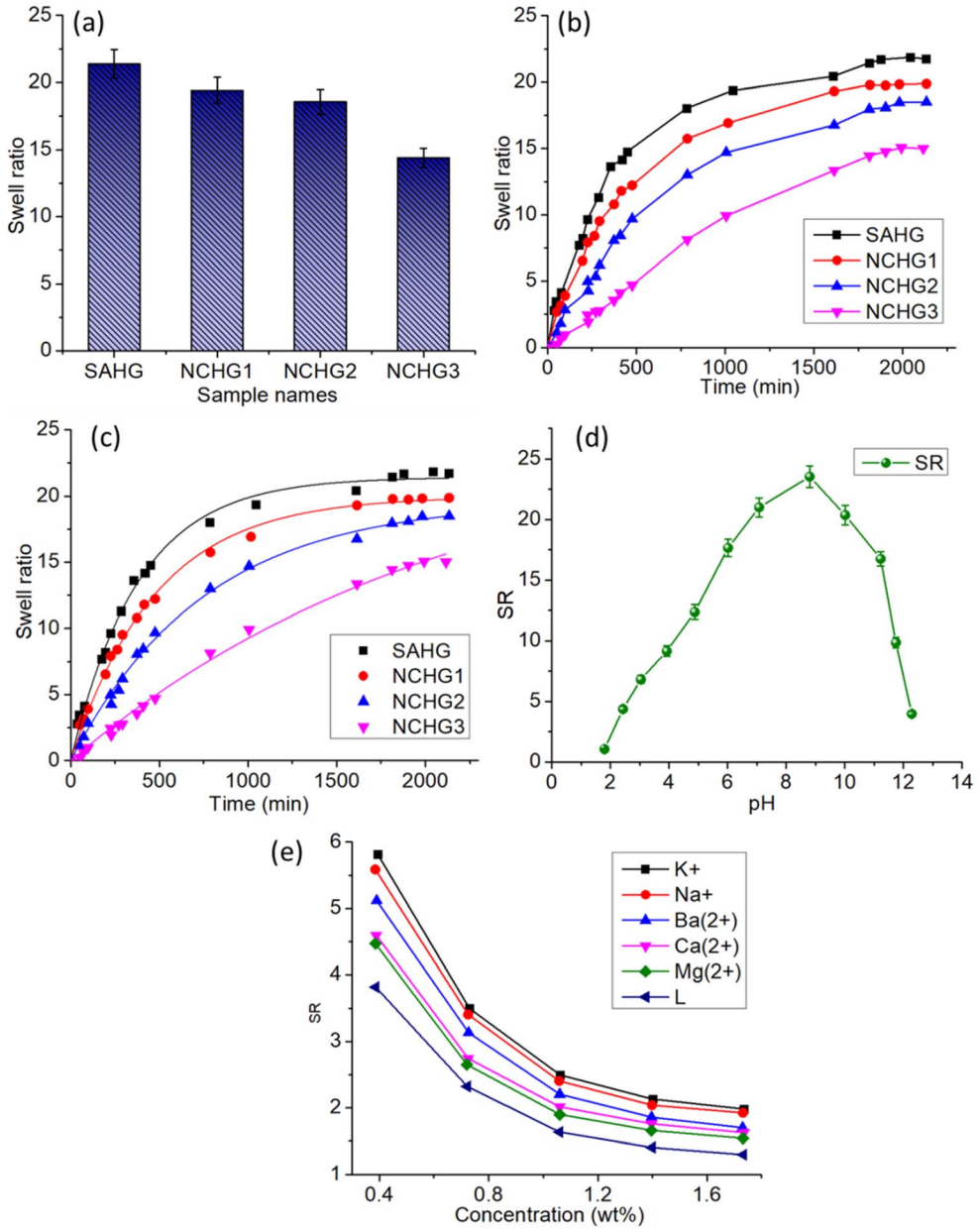

Fig. 7 (a) Water uptake behavior of the unfilled hydrogel (SAHG) and other MMT loaded nanocomposite hydrogels (NCHG1, NCHG2, and NCHG3). (b) Time-dependent water uptake behavior of the prepared hydrogels. (c) 1st order rate kinetic equation fittings into the time-dependent water uptake data of the hydrogels. (d) pH-responsive water uptake behavior of the NCHG2 hydrogel. (e) Effect of medium salinity to water uptake (swelling) behavior of the nanocomposite hydrogel (NCHG2).

that restricts polymer chain mobility while maintaining flexibility.[66] The compressive stress–strain plot (Fig. 8b) further illustrates the mechanical reinforcement effect. The SAHG displayed the lowest compressive stress, reaching ~0.10 MPa at 80% strain. In contrast, NCHG3 exhibited the highest compressive stress (~0.15 MPa), signifying improved resistance to deformation under compression. This enhancement arises from the synergistic effect of polyacrylamide-functionalized polysaccharides, which provide a robust hydrogen-bonding network, and the dispersed MMT nanoparticles, which serve as mechanical reinforcements.[67] The presence of the semi-IPN structure effectively dissipates stress, contributing to enhanced load-bearing capacity. The enhanced mechanical strength is crucial for maintaining the structural integrity of the hydrogel during pH-responsive drug release. The reinforced network ensures that the hydrogel maintains its three-dimensional structure in acidic or alkaline environments, preventing premature swelling or collapse. This stability is particularly beneficial for controlled drug delivery systems targeting nootropic and neuroprotective agents, as the hydrogel can sustain prolonged release while protecting encapsulated bioactive molecules.

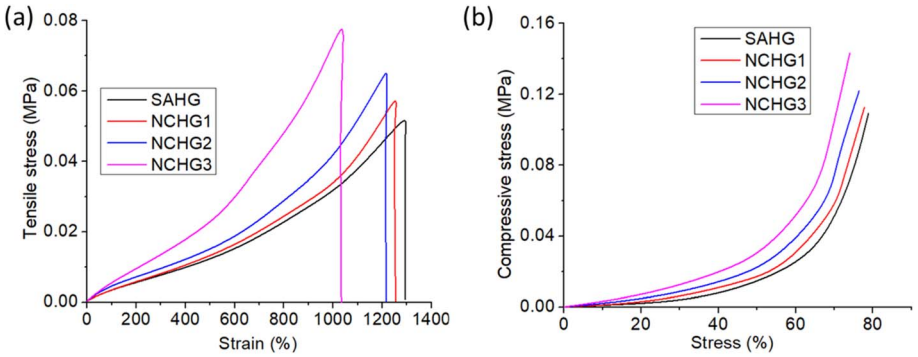

Fig. 8 (a) Tensile stress–strain plot of pure hydrogel and MMT loaded nanocomposite hydrogel. (b) Compressive stress–strain plot of pure hydrogel and MMT loaded nanocomposite hydrogel.

Drug release behavior and kinetics

The drug release behavior of the polyacrylamide-functionalized polysaccharide-based nanocomposite hydrogels was evaluated at two different temperatures, 37 °C and 44 °C, to simulate physiological and elevated temperature conditions, respectively. The cumulative drug release profiles and corresponding Korsmeyer–Peppas model fittings are presented in Fig. 9. At 37 °C (Fig. 9a and b), the pure hydrogel (SAHG) exhibited the highest cumulative drug release (~70% after 300 min), while the nanocomposite hydrogels (NCHG1, NCHG2, and NCHG3) demonstrated progressively reduced drug release rates. Drug release studies were performed at 37 °C and 44 °C to simulate normal and hyperthermic physiological conditions, respectively. The temperature of 37 °C corresponds to the core body temperature and represents drug release under normal physiological state. The elevated temperature of 44 °C was selected to mimic febrile or hyperthermic conditions, which are commonly reported in neurological disorders such as ischemic stroke, traumatic brain injury, and central nervous system infections. Hyperthermia is known to aggravate neuronal injury, and therefore, evaluating the drug release behavior under such conditions is important to understand the potential performance of the hydrogel in pathological states. NCHG3 displayed the lowest release (~55% after 300 min), indicating a strong network structure that restricts drug diffusion. This trend is attributed to the increased MMT content, which

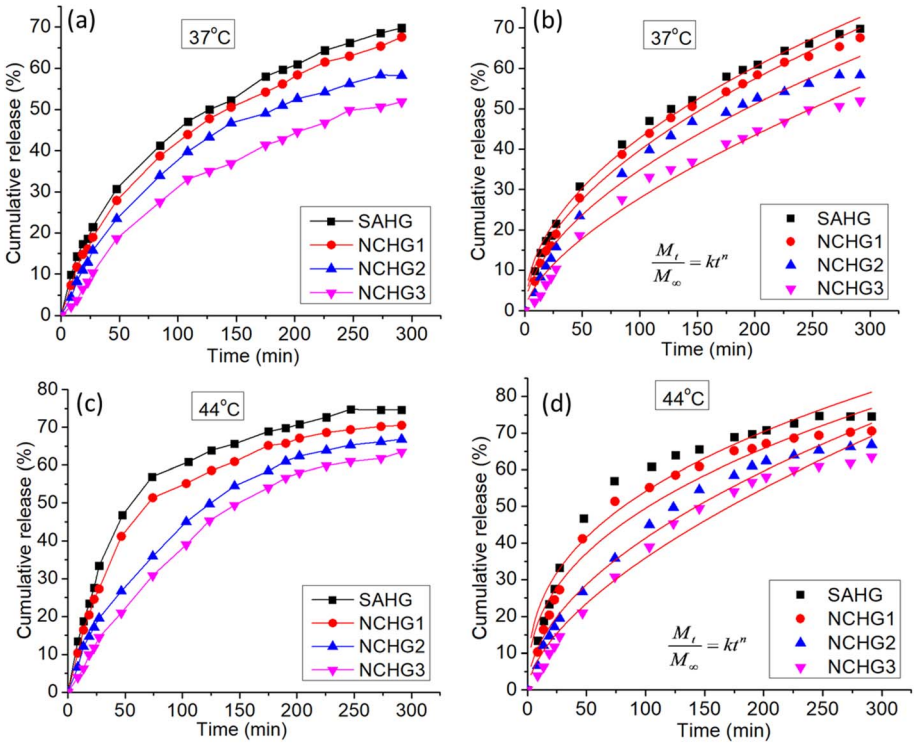

Fig. 9 (a) Cumulative drug release study of the hydrogels at 37 °C. (b) Korsmeyer–Peppas model fitting plot of the drug release at 37 °C. (c) Cumulative drug release study of the hydrogels at 44 °C. (d) Korsmeyer–Peppas model fitting plot of the drug release at 44 °C

reinforces the hydrogel matrix, resulting in denser crosslinking and reduced free volume for molecular diffusion. At 44 °C (Fig. 9c and d), a similar trend was observed, with SAHG exhibiting the highest release (~75%) and NCHG3 showing the lowest (~60%). The elevated temperature enhanced polymer chain mobility and water uptake, promoting faster drug diffusion. However, the presence of MMT nanoparticles in the nanocomposite hydrogels still mitigated excessive release by reinforcing the network structure.

To further understand the drug release mechanism, the data were fitted to the Korsmeyer–Peppas model:[68]

$$\frac{M_t}{M_\infty} = kt^n \quad (1)$$

where M_t and M_∞ correspond to the amount of drug released at time 't' and total amount of drug released at infinite time respectively. 'k' and 'n' signify kinetic constant reflecting structural and geometric characteristics and release exponent indicating the drug release mechanism, respectively.

From the model fitting plots (Fig. 9b and d), the obtained n-values provide insight into the release mechanisms as follows:

For SAHG, $n \approx 0.54$ at 37 °C and $n \approx 0.51$ at 44 °C indicating non-Fickian diffusion (anomalous transport) where both diffusion and polymer relaxation influence drug release. For NCHG1, $n \approx 0.48$ at 37 °C and $n \approx 0.45$ at 44 °C suggesting a transition toward Fickian diffusion, where the release is diffusion-controlled with minimal polymer relaxation effects. For NCHG2 and NCHG3, $n \approx 0.42$ and $n \approx 0.39$ at 37 °C and 44 °C, respectively, indicating a strong shift toward Fickian diffusion, consistent with restricted polymer chain dynamics due to the presence of higher MMT content. The decreasing n-values with increasing MMT content confirm that nanocomposite incorporation effectively suppresses polymer chain relaxation, reinforcing a diffusion-controlled release pattern.[69] This behavior is advantageous for sustained drug delivery, particularly in controlled-release systems targeting prolonged therapeutic efficacy. The analysis highlights that the introduction of MMT

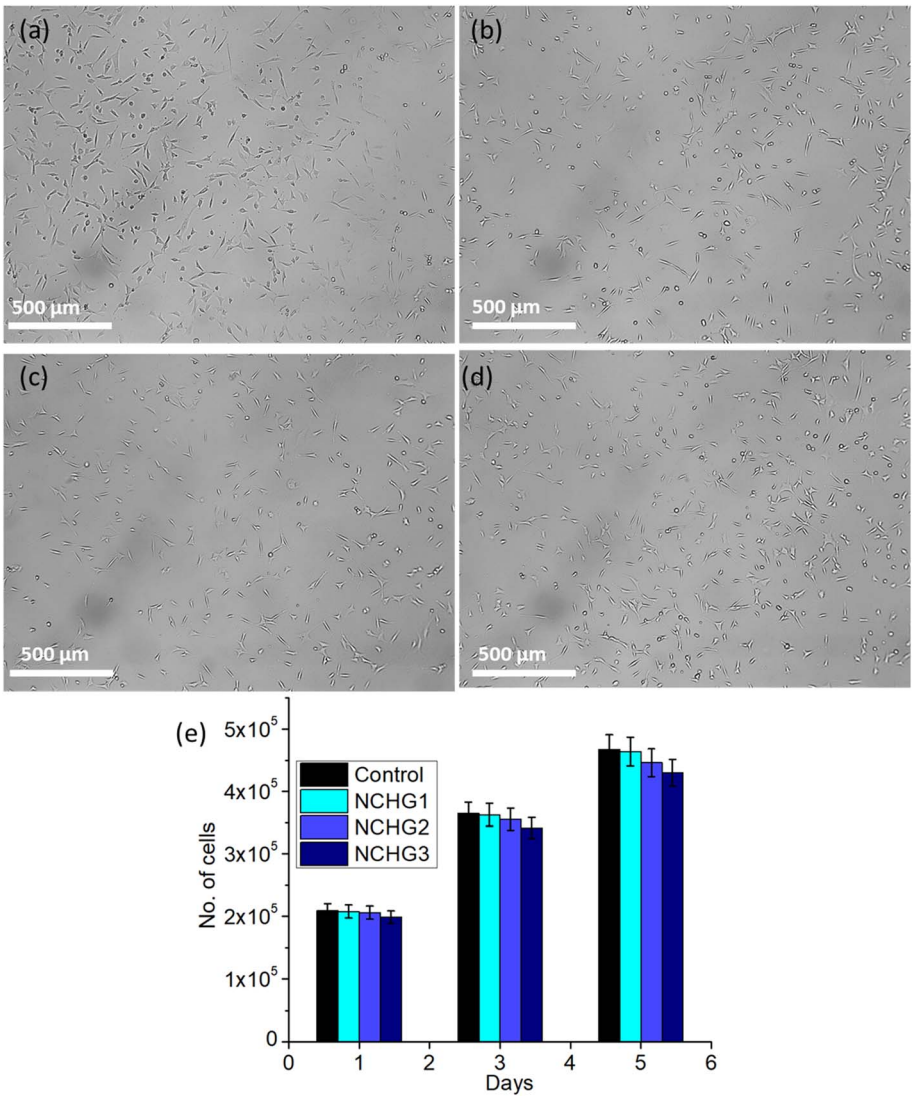

Fig. 10 Cell (fibroblasts 3T3) proliferation test under optical microscope for (a) control (b) NCHG1 (c) NCHG2 and (d) NCHG3. (e) Cell proliferation histogram of the hydrogels and their comparison with the control.

nanoparticles significantly influences the hydrogel's network structure, reducing drug diffusion rates and shifting the release mechanism toward Fickian diffusion.[70] The Korsmeyer–Peppas model fitting further supports this conclusion, with decreasing *n*-values correlating with the densification of the hydrogel matrix.[71] These findings demonstrate the potential of polyacrylamide-functionalized polysaccharide-based nanocomposite hydrogels as robust drug delivery platforms, offering controlled release profiles suitable for biomedical applications.

The cumulative drug release profiles at pH 4.2 and pH 8.6 clearly demonstrate the pH-responsiveness of the hydrogel systems. At pH 4.2 (Fig. S1), all hydrogels (SAHG, NCHG1–3) exhibited a relatively slow and sustained release, with cumulative release values reaching approximately 50–60% after 300 minutes. Among them, SAHG showed the highest release, followed by NCHG1, NCHG2, and NCHG3, indicating that the degree of network modification influences diffusion rates. In contrast, at pH 8.6 (Fig. S2), the release was noticeably faster, with cumulative release values approaching 70–80% within the same time frame. This pronounced increase in release rate under alkaline conditions suggests that deprotonation of ionizable groups (likely –COOH groups in the polymer matrix) leads to stronger electrostatic repulsion, network expansion, and enhanced drug diffusion. The difference in release kinetics between the two pH conditions highlights that the hydrogels are more stable and provide better control of drug delivery in acidic environments, whereas alkaline conditions promote a burst release behavior. These observations confirm that the network architecture and pH sensitivity of the hydrogels play a key role in modulating drug release kinetics.

Cytotoxicity evaluation against living cells

The cytotoxicity assessment of the developed polyacrylamide-functionalized polysaccharide-based nanocomposite semi-interpenetrating polymeric network (semi-IPN) hydrogel was conducted using fibroblast 3T3 cells. Fig. 10(a–d) shows the optical microscopic images of 3T3 fibroblasts cultured for 3 days on the control surface and on hydrogel samples NCHG1, NCHG2, and NCHG3. The images indicate that cells adhered well and exhibited normal morphology on all hydrogel samples, comparable to the control. A gradual increase in cell density is observed across NCHG1 to NCHG3, suggesting that the hydrogel formulations support cell proliferation and are cytocompatible. These observations are consistent with the quantitative cell viability results, confirming that the nanocomposite hydrogels do not exert cytotoxic effects. The cell proliferation histogram shown in Fig. 10e illustrates the growth pattern of fibroblasts over five days in the presence of the hydrogel formulations (NCHG1, NCHG2, and NCHG3) compared to the control. On day 1, all hydrogel samples exhibited cell counts comparable to the control group, suggesting no immediate cytotoxic effects. Over the following days, cell proliferation showed a consistent upward trend across all groups. By day 3, the cell population increased significantly for all samples, with cell counts approaching those of the control group. This demonstrates that the hydrogel materials supported cell viability and proliferation without exerting any inhibitory effects. By day 5, the cell counts in the hydrogel groups (NCHG1, NCHG2, and NCHG3) were slightly lower but statistically comparable to the control, confirming that the hydrogel formulations maintained a biocompatible environment conducive to cell growth.[72] The observed results indicate that the polyacrylamide-functionalized polysaccharide-based semi-IPN hydrogel exhibits excellent cytocompatibility, which is crucial for biomedical applications such as drug delivery. The consistent cell proliferation pattern highlights the non-toxic nature of the hydrogel system, reinforcing its suitability as a potential carrier for pH-responsive nootropic and neuroprotective drug delivery systems.

Conclusions

In this study, a polyacrylamide-functionalized polysaccharide-based nanocomposite semi-interpenetrating polymeric network (semi-IPN) hydrogel was successfully developed for pH-responsive nootropic and neuroprotective drug delivery. The hydrogel exhibited high mechanical strength, ensuring structural stability for prolonged use. Its pH-responsive behavior enabled controlled drug release, demonstrating potential for targeted delivery applications. SEM analysis revealed a porous architecture that enhanced water absorption, drug loading, and diffusion, while XRD confirmed the hydrogel's semi-crystalline structure, contributing to its improved mechanical stability. Additionally, fibroblast 3T3 cell proliferation studies demonstrated excellent biocompatibility with no observed cytotoxicity. These findings highlight the hydrogel's potential as a multifunctional platform for controlled drug delivery in neuroprotective therapies. Further investigations may focus on optimizing the formulation for enhanced *in vivo* performance. By integrating artificial intelligence with hydrogel-based systems, future advancements in brain-targeted drug delivery could enhance therapeutic outcomes, reduce side effects, and improve neuroprotection.

Author contributions

Nada H. Aljarba, and Saad Alkahtani: scientific and technical discussion, Mohd Afzal: formal analysis, investigation, and interpretation of data. Mohd Afzal and Mariam Alkhateeb: data curation, formal analysis, investigation, writing review, and editing. Mohd Afzal and Nada H. Aljarba: substantial contribution to conceptualization, methodology, drafting, designing, acquisition, analysis, interpretation of data, and writing – review and editing the article.

Conflicts of interest

The authors declare no conflict of interest.

Data availability

The data that support the findings of this study are available on request from the corresponding author.

Supplementary information is available. See DOI: https://doi.org/10.1039/d5ra06115f.

Acknowledgements

This research was funded by the Deanship of Scientific Research and Libraries at Princess Nourah bint Abdulrahman University, Riyadh through the Research Funding Program, Grant No. (FRP-2025-25).

References

1 H. Mittal, S. S. Ray and M. Okamoto, *Macromol. Mater. Eng.*, 2016, **301**, 496–522.
2 Z. Li and Z. Lin, *Aggregate*, 2021, **2**, e21.
3 S. Ganguly, D. Ray, P. Das, P. P. Maity, S. Mondal, V. Aswal, S. Dhara and N. C. Das, *Ultrason. Sonochem.*, 2018, **42**, 212–227.
4 S. Ganguly, T. K. Das, S. Mondal and N. Das, *RSC Adv.*, 2016, **6**, 105350–105362.
5 P. Das, S. Ganguly, P. K. Marvi, M. Sherazee, S. R. Ahmed, X. Tang, S. Srinivasan and A. R. Rajabzadeh, *Adv. Funct. Mater.*, 2024, 2314520.
6 P. Das, S. Ganguly, A. Saravanan, S. Margel, A. Gedanken, S. Srinivasan and A. R. Rajabzadeh, *ACS Appl. Bio Mater.*, 2022, **5**, 5617–5633.
7 R. Jaiswal and A. P. Sherje, *J. Drug Delivery Sci. Technol.*, 2024, 105990.
8 A. Manzoor, A. H. Dar, V. K. Pandey, R. Shams, S. Khan, P. S. Panesar, J. F. Kennedy, U. Fayaz and S. A. Khan, *Int. J. Biol. Macromol.*, 2022, **213**, 987–1006.
9 S. Selvaraj, A. Chauhan, V. Dutta, R. Verma, S. K. Rao, A. Radhakrishnan and S. Ghotekar, *Int. J. Biol. Macromol.*, 2024, 130991.
10 P. Das, S. Ganguly, S. R. Ahmed, M. Sherazee, S. Margel, A. Gedanken, S. Srinivasan and A. R. Rajabzadeh, *ACS Appl. Polym. Mater.*, 2022, **4**, 9323–9340.
11 H. Zhang, S. Su, S. Liu, C. Qiao, E. Wang, H. Chen, C. Zhang, X. Yang and T. Li, *Molecules*, 2023, **28**, 5211.
12 H. Khalil, Y. Tye, C. Saurabh, C. Leh, T. Lai, E. Chong, M. N. Fazita, J. M. Hafiidz, A. Banerjee and M. Syakir, *eXPRESS Polym. Lett.*, 2017, **11**, 244–265.
13 P. Das, M. Sherazee, P. K. Marvi, S. R. Ahmed, A. Gedanken, S. Srinivasan and A. R. Rajabzadeh, *ACS Appl. Mater. Interfaces*, 2023, **15**, 29425–29439.
14 P. Das, S. Ganguly, P. K. Marvi, M. Sherazee, X. Tang, S. Srinivasan and A. R. Rajabzadeh, *Adv. Mater.*, 2024, **36**, 2409819.
15 S. Ganguly, P. Das, S. Srinivasan, A. R. Rajabzadeh, X. S. Tang and S. Margel, *ACS Appl. Nano Mater.*, 2024, **7**, 5272–5286.
16 S. Ganguly and N. C. Das, *RSC Adv.*, 2015, **5**, 18312–18327.
17 S. Ganguly and S. Margel, *Prog. Polym. Sci.*, 2022, **131**, 101574.
18 A. Roy, P. Chakraborty and P. Das, *Biomass Convers. Biorefin.*, 2024, 1–16.
19 Z. Zhang, H. Li, M. Qian, Y. Zheng, L. Bao, W. Cui and D. Wang, *Regener. Biomater.*, 2025, **12**, rbaf004.
20 C. Song, R. Liu, B. Kong, Z. Gu and G. Chen, *Biomed. Technol.*, 2024, **5**, 73–81.
21 F. Lin, Y. Li and W. Cui, *Biomed. Technol.*, 2023, **1**, 18–29.
22 Y. Xu, Y. Zhou, S. Meng, C. Zhou, N. Yang, L. Bao and W. Lu, *Biomed. Mater.*, 2025, **20**, 035015.
23 Y. Zhao, Z. S. Zhu, J. Guan and S. J. Wu, *Acta Biomater.*, 2021, **125**, 57–71.
24 W. Xing and Y. Tang, *Nano Mater. Sci.*, 2022, **4**, 83–96.
25 Z. Chen, J. Tang, N. Zhang, Y. Chen, Y. Chen, H. Li and H. Liu, *Colloids Surf., A*, 2022, **633**, 127867.
26 F. Khan, M. Atif, M. Haseen, S. Kamal, M. S. Khan, S. Shahid and S. A. Nami, *J. Mater. Chem. B*, 2022, **10**, 170–203.
27 S. Bashir, M. Hina, J. Iqbal, A. Rajpar, M. Mujtaba, N. Alghamdi, S. Wageh, K. Ramesh and S. Ramesh, *Polymers*, 2020, **12**, 2702.
28 T. Wang, W. Zhao, Y. Wu, X. Wang, A. B. Kayitmazer, A. Ahmad, N. Ramzan, Y. Si, J. Wang and Y. Xu, *ACS Appl. Polym. Mater.*, 2023, **5**, 1169–1179.
29 Z. Wu, X. Liu, Q. Xu, L. Zhang, S. N. Abdou, M. M. Ibrahim, J. Zhang, Z. M. El-Bahy, N. Guo and J. Gao, *J. Polym. Sci.*, 2024, **62**, 4599–4611.
30 C. Feng, L. Cai, G. Zhu, L. Chen, X. Xie and J. Guo, *J. Colloid Interface Sci.*, 2025, **677**, 692–703.
31 C. Feng, B. Xu, W. Luo, H. Liao, Z. Qiu and J. Guo, *Colloids Surf., A*, 2024, **703**, 135324.
32 S. Ganguly, D. Wulff, C.-M. Phan, L. W. Jones and X. S. Tang, *ACS Appl. Bio Mater.*, 2024, **7**, 6286–6296.
33 N. Zoratto and P. Matricardi, *Polym. Gels*, 2018, 91–124.
34 L. Chikh, V. Delhorbe and O. Fichet, *J. Membr. Sci.*, 2011, **368**, 1–17.
35 M. Wang, J. Jiang, S. Liang, C. Sui and S. Wu, *Macromol. Rapid Commun.*, 2024, **45**, 2400539.
36 S. Ganguly, P. Das, P. P. Maity, S. Mondal, S. Ghosh, S. Dhara and N. C. Das, *J. Phys. Chem. B*, 2018, **122**, 7201–7218.
37 P. Tiwari, S. Bhardwaj, S. Singh and P. K. Maji, *Polym. Adv. Technol.*, 2024, **35**, e6556.
38 S. Abrishami and Z. Maghsoud, *Polymer*, 2024, **311**, 127561.
39 K. Sendrowski, W. Sobaniec, A. Stasiak-Barmuta, P. Sobaniec and J. Popko, *Pharmacol. Rep.*, 2015, **67**, 326–331.
40 J. M. Brimson, S. Brimson, M. I. Prasanth, P. Thitilertdecha, D. S. Malar and T. Tencomnao, *Sci. Rep.*, 2021, **11**, 596.
41 K. Koshibu, *Neural Regener. Res.*, 2016, **11**, 79–80.
42 A. D. Gholap, M. J. Uddin, M. Faiyazuddin, A. Omri, S. Gowri and M. Khalid, *Comput. Biol. Med.*, 2024, 108702.
43 (*a*) A. Blanco-González, A. Cabezón, A. Seco-González, D. Conde-Torres, P. Antelo-Riveiro, Á. Piñeiro and R. Garcia-Fandino, *Pharmaceuticals*, 2023, **16**, 891; (*b*) S. Singh, N. Kaur and A. Gehlot, *Comput. Biol. Med.*, 2024, **179**, 108810.
44 B. Hoseini, M. R. Jaafari, A. Golabpour, Z. Rahmatinejad, M. Karimi and S. Eslami, *Curr. Drug Delivery*, 2025, **22**, 1287.
45 J. Fitzgerald, D. Higgins, C. M. Vargas, W. Watson, C. Mooney, A. Rahman, N. Aspell, A. Connolly, C. A. Gonzalez and W. Gallagher, *J. Clin. Pathol.*, 2021, **74**, 429–434.
46 S. Gardner, S. Das and K. Taylor, in *Artificial Intelligence in Oncology Drug Discovery and Development*, IntechOpen, 2020.

47 L. Liu, W. Yao, Y. Rao, X. Lu and J. Gao, *Drug Delivery*, 2017, **24**, 569–581.
48 Z. Zhang, L. Lu, B. Hong, Q. Ye, L. Guo, C. Yuan, B. Liu and B. Cui, *Carbohydr. Polym.*, 2025, **347**, 122783.
49 F. Zhu, Y. Hu, L. Meng, W. Li, B. Xie, Z. Zhou, S. Cui, M. Wang, Y. Wang and Z. Chen, *Int. J. Biol. Macromol.*, 2024, **278**, 134692.
50 S. Ganguly, P. Bhawal, A. Choudhury, S. Mondal, P. Das and N. C. Das, *Polym.-Plast. Technol. Eng.*, 2018, **57**, 997–1014.
51 Y. Wu, S. Ganguly and X. S. Tang, *Int. J. Bioprint.*, 2024, **10**, 1637.
52 Y. N. Zhang, J. Y. Cui and S. A. Xu, *Starch/Staerke*, 2015, **67**, 949–957.
53 M. M. Ghobashy, H. Abd El-Wahab, M. A. Ismail, A. Naser, F. Abdelhai, B. K. El-Damhougy, N. Nady, A. S. Meganid and S. A. Alkhursani, *J. Mater. Sci. Eng. B*, 2020, **260**, 114645.
54 B. Zhu, D. Ma, J. Wang and S. Zhang, *Carbohydr. Polym.*, 2015, **133**, 448–455.
55 D. Ma, B. Zhu, B. Cao, J. Wang and J. Zhang, *J. Macromol. Sci., Part B:Phys.*, 2016, **55**, 1124–1133.
56 S. Ganguly, P. Das, T. K. Das, S. Ghosh, S. Das, M. Bose, M. Mondal, A. K. Das and N. C. Das, *Ultrason. Sonochem.*, 2020, **60**, 104797.
57 X. Bao, L. Yu, S. Shen, G. P. Simon, H. Liu and L. Chen, *Carbohydr. Polym.*, 2019, **219**, 395–404.
58 X. Bao, L. Yu, G. P. Simon, S. Shen, F. Xie, H. Liu, L. Chen and L. Zhong, *Carbohydr. Polym.*, 2018, **192**, 1–9.
59 R. Singh and V. Mahto, *Pet. Sci.*, 2017, **14**, 765–779.
60 A. M. Nzenguet, M. Aqlil, Y. Essamlali, O. Amadine, A. Snik, M. Larzek and M. Zahouily, *J. Polym. Res.*, 2018, **25**, 1–13.
61 R. da Silva Fernandes, M. R. de Moura, G. M. Glenn and F. A. Aouada, *J. Mol. Liq.*, 2018, **265**, 327–336.
62 S. D. Chaudhuri, A. Dey, S. Upganlawar and D. Chakrabarty, *Mater. Chem. Phys.*, 2022, **282**, 125942.
63 H. Mittal, A. Al Alili and S. M. Alhassan, *Appl. Clay Sci.*, 2022, **230**, 106712.
64 S. A. Khan and T. A. Khan, *J. Environ. Chem. Eng.*, 2021, **9**, 105575.
65 S. Ganguly and N. C. Das, *Polym.-Plast. Technol. Eng.*, 2017, **56**, 744–761.
66 T. Li, X. Zhang, B. Xia, P. Ma, M. Chen, M. Du, Y. Wang and W. Dong, *New J. Chem.*, 2020, **44**, 16569–16576.
67 Z. Guo, Y. Bi, Z. Wu and C. Yuan, *Wear*, 2025, 205786.
68 A. Talevi and M. E. Ruiz, in *The ADME Encyclopedia: A Comprehensive Guide on Biopharmacy and Pharmacokinetics*, Springer, 2022, pp. 613–621.
69 T. D. Stocco, A. M. H. da Silva, S. G. C. de Paula e Silva and A. O. Lobo, in *Fiber and Ceramic Filler-Based Polymer Composites for Biomedical Engineering*, Springer, 2024, pp. 193–216.
70 S. Argin, P. Kofinas and Y. M. Lo, *Food Hydrocolloids*, 2014, **40**, 138–144.
71 S. Owonubi, B. Aderibigbe, E. Mukwevho, E. Sadiku and S. S. Ray, *Int. J. Ind. Chem.*, 2018, **9**, 39–52.
72 R. Rivero, F. Alustiza, V. Capella, C. Liaudat, N. Rodriguez, P. Bosch, C. Barbero and C. Rivarola, *Colloids Surf., B*, 2017, **158**, 488–497.